Applied Radiation and Isotopes 202 (2023) 111069

Contents lists available at ScienceDirect

Applied Radiation and Isotopes

journal homepage: www.elsevier.com/locate/apradiso

Identification of defect centers responsible for thermoluminescence emission in sol-gel synthesized calcium silicate phosphor

Zaida V. Vilca [a,**], T.K. Gundu Rao [a], René R. Rocca [b], J.F. Benavente [c], Joseff R. Mejia-Bernal [d], José F.D. Chubaci [e], Betzabel N. Silva-Carrera [e], Jorge S. Ayala-Arenas [a], Nilo F. Cano [b,*]

[a] Universidad Nacional de San Agustín de Arequipa - UNSA, Arequipa, Peru
[b] Universidade Federal de São Paulo, Instituto do Mar, Santos, SP, Brazil
[c] CIEMAT, Av. Complutense 40, E, 28040, Madrid, Spain
[d] Universidad de Guanajuato, División de Ciencias e Ingenierías, León, Guanajuato, Mexico
[e] Universidade de São Paulo, Instituto de Física, São Paulo, SP, Brazil

ARTICLE INFO

Keywords:
Calcium silicate
TL
EPR
Defect centers

ABSTRACT

The thermoluminescence (TL) of calcium silicate phosphor (CSO) prepared by the sol-gel method and sintered at 1200 °C were investigated. From Tm-Tstop curve, TL emission spectrum and computer deconvolution using electron traps with discrete and continuous distributions, the glow curves were found to be composed of four TL peaks (117, 190, 250 and 275 °C) with a single emission band centered at 370 nm. Electron paramagnetic resonance (EPR) investigation has been carried out to identify the defect centers formed in the CSO phosphor by γ-irradiation and find the centers related to the TL process in the phosphor. At room temperature, three defect centers were observed. The first center, characterized by the principal *g*-values of 2.014, 2.011, and 2.0080 was assigned to an O^- ion. The second center with *g*-values 2.015, 2.013, and 2.010 is also attributed to an O^- ion and is associated with the TL peak at 280 °C. The third center, with an isotropic *g*-value of 2.0011 was identified as the F^+ center (singly ionized oxygen vacancy) and relates to the TL peak at 280 °C.

1. Introduction

Dosimetry plays a fundamental role in all irradiation processes since it makes it possible to ensure acceptable dose levels in a radiation exposure procedure, establishing radiological protection for the environment and for the individual. Therefore, the search for new materials with suitable properties to measure the radiation dose continues to be of scientific interest for dosimetry.

Radiation absorbed by a material medium produces ionization. Part of the absorbed energy is transformed into heat, while a fraction causes the breaking of chemical bonds. In some solid materials, part of the energy of the absorbed radiation is stored in metastable energy states within the forbidden band by capturing charge carriers (free electrons and holes). These metastable states are due to the presence of imperfections (intrinsic, extrinsic, structural, etc.) in the crystal lattice of the material, formed during the synthesis process of the crystalline material. When the material is stimulated with heat, the charge carriers are released from their trapping centers, resulting in the emission of thermoluminescence (TL) light after recombination (McKeever, 1985). Therefore, a study of the TL properties and the elucidation of the defect centers responsible for the luminescent emission of a material is essential to determine the TL properties and to understand the charge capture and recombination mechanisms leading to the TL light emission process. This understanding allows us to establish the suitability of a material for a given application in radiation dosimetry. The identification of the defect centers responsible for trapping and luminescence emissions in a material is not straightforward. In fact, the studies of TL give only a phenomenological picture, while the possibility of comparing the electron paramagnetic resonance (EPR) features as a function of irradiation and thermal treatments with the luminescence properties can allow determining which are the centers responsible for them (Marfunin, 1979).

In a TL glow curve as a function of temperature, the position of the peaks can be associated with the energy levels of the traps. The behavior of the TL glow curve of a material as a function of the dose is associated with the processes of charge carrier transfer both in the irradiation stage

* Corresponding author. Universidade Federal de São Paulo, Instituto do Mar, Santos, SP, Brazil.
** Corresponding author. Universidad Nacional de San Agustín de Arequipa - UNSA, Arequipa, Peru.
E-mail addresses: zvilcav@unsa.edu.pe (Z.V. Vilca), nilocano@if.usp.br, nilo.cano@unifesp.br (N.F. Cano).

https://doi.org/10.1016/j.apradiso.2023.111069
Received 27 July 2023; Received in revised form 4 October 2023; Accepted 9 October 2023
Available online 11 October 2023

and in the heating process during the TL readout and can provide evidence of the existence of competition processes between defects for the capture of charge carriers. These TL glow curves obtained have to be studied using correct correlation between experimental methodologies and numerical tools, using mathematical models that only can give accurate results if these are based on empirical data. This strong correlation has been evaluated using numerical simulations, which reproduces realistic TL materials behavior during both irradiation and heating stages (Benavente et al., 2021). Therefore, a wide-ranging set of experimental techniques, based on TL properties can be used to obtain all the kinetic parameters (E, s, T_{Max}, I_{Max}, b and σ) related to each distribution. These methods include the Initial Rise (IR) and the Variable Heating Rate (VHR) methods, which are only effective when these contributions do not overlap. Otherwise, only deconvolution techniques can give optimal results. However, in this case, the mathematical model used to fit the experimental data must be as precise as possible, trying to reduce the possible systematic error of the model as much as possible. Therefore, the well-interpreted Tm-Tstop method facilitates the correlation of mathematical models with the contributions of the TL material.

Similarly, in a measurement of TL intensity as a function of wavelength (λ), spectral bands can be associated with the recombination centers responsible for TL emission. In this way, we can interpret the charge transfer mechanisms during the recombination process that gives rise to TL light. Therefore, the TL emission spectrum of a phosphor, with emission band(s) centered at a wavelength (λ), and others, if any, indicate the number of recombination centers involved during TL emission.

Among the solid luminescent materials with interesting dosimetric characteristics for ionizing and non-ionizing radiation dosimetry are the silicates (Cano et al., 2023; Watanabe et al., 2015; Barbosa et al., 2014), among which we can highlight calcium silicate.

Calcium silicate, also known as wollastonite, exists in two structurally distinct forms. The high-temperature form, called pseudo-wollastonite, has a triclinic crystal structure. On the other hand, the low-temperature form can have two different structures: wollastonite-2M, which has a monoclinic symmetry, or wollastonite-Tc, which has a triclinic symmetry. Wollastonite-2M has a chain silicate structure, with a repeat unit containing three silicon-oxygen tetrahedra. The oxygen atoms coordinate with the calcium atom to form an approximate octahedron. Wollastonite-M, on the other hand, has a perovskite structure with a space group of $P2/c$. Three bridging oxygens connect the silicon tetrahedra in this structure, while six non-bonding oxygens only connect to one silicon atom. The structure of wollastonite-M has been refined by Hesse (1984).

The TL properties of natural and synthetic calcium silicate doped with different impurities were studied in some detail by several researchers (Souza et al., 2007a; Souza et al., 2007b; Gonzales-Lorenzo et al., 2018; Gonzales-Lorenzo et al., 2020; Gonzales-Lorenzo et al., 2021; Kulkarni et al., 2011; Jain et al., 2022; Nijalingappa et al., 2020; Palan et al., 2016. However, no serious attempt has been made to identify the defect centers responsible for the TL emission of pure calcium silicate.

In the present study, we have studied the TL properties of calcium silicate (CSO) produced by the sol-gel process. In addition, we have reported the results of EPR studies of CSO and tried to correlate the EPR results with TL results for a possible explanation of the defect centers responsible for the TL emission. The main motivation for this study is related to the importance that luminescent signals play in dosimetry. Consequently, a better understanding of the physical mechanisms and centers involved is of great importance both from a theoretical point of view and for dosimetric applications of this material.

2. Experimental details

2.1. Synthesis

Calcium silicate (CSO) phosphor was synthesized by the sol-gel process. All chemicals and reagents are of analytical grade and used without any further purification. The starting materials are calcium nitrate tetrahydrate ($CaN_2O_6 \bullet 4H_2O$) (99% Sigma-Aldrich), tetraethyl orthosilicate (TEOS) ($C_8H_{20}O_4Si$) (99% Sigma-Aldrich), nitric acid (HNO_3) (53% Delta Química) as the catalyst, 2-propanol (98.9% Sigma-Aldrich), and distilled water. For the preparation, a stoichiometric amount of TEOS was mixed with a sufficient amount of 2-propanol in a magnetic plate with constant stirring (solution A). On the other hand, stoichiometric amounts of $CaN_2O_6 \bullet 4H_2O$ are dissolved in distilled water with constant stirring on a magnetic hot plate at 70 °C for 30 min (solution B). Finally, solution A was added to solution B at 70 °C, in addition to adding a few drops of HNO_3, this whole process of calcium silicate sol-gel formation was carried out with continuous stirring for 1h at 70 °C. Finally, for the drying process of the sol-gel sample, it was kept in a furnace at 70 °C for 48 h. The dried sample was ground using an agate mortar and proceeded to separate into three groups for sintering at 1100, 1200, and 1300 °C for 2 h, respectively. The desired sintering (1100, 1200 and 1300 °C) for 2 h was performed at a heating rate of 3 °C/min using a high-temperature furnace, followed by cooling to room temperature by shutting the furnace. The sintered samples were further ground for X-ray diffraction (XRD) measurements and compacted and sintered pellets were produced for TL measurements.

2.2. Instrumentation

2.2.1. X-ray diffraction

The crystalline structure of the calcined samples was characterized by XRD using a Rigaku MiniFlex 600 laboratory diffractometer with Ni-filtered Cu-Kα radiation at 40 kV and 15 mA, with a scanning step of 0.02 in the 2θ range from 10 to 60, and analyzed with the X'pert HighScore Plus software.

2.2.2. Thermoluminescence

In this study, the CSO samples were first pressed into 5 mm diameter and 1 mm thick tablets using a mass of 50 mg. Prior to TL measurement, the pressed samples were calcined at 1100, 1200, and 1300 °C for 2 h to study the effect of sintering temperature on the pellets. The TL glow curves were recorded using two Harshaw TL reader systems (models 3500 and 4500), both readers equipped with a Hamamatsu bi-alkaline photomultiplier tube (PMT) for light detection. A filter with a transmission band between 330 and 690 nm was used in front of the PMT. The TL measurements were carried out in a nitrogen atmosphere in the temperature range of 50–400 °C with a heating rate of 4 °C/s. For each glow curve, five measurements were performed using the same pellet. The incandescent background signal was directly subtracted from the TL data. The TL emission spectrum measurements were carried out on the same Risø TL/OSL readout by connecting a monochromator in front of the detection system.

2.2.3. Electron paramagnetic resonance

EPR spectra of the powdered sample were recorded at room temperature on a MiniScope 5000 EPR spectrometer of Bruker operating at the X-band frequency (9.50053 GHz) with a 100 kHz field modulation, microwave power of 20 mW and using an average sample mass of 150 mg. Powder samples were filled in quartz capillary tubes and placed inside the EPR cavity.

2.3. Irradiation

The CSO samples were irradiated with two ^{60}Co γ-ray sources. For low doses in the region of mGy to Gy, the samples were irradiated with a

source irradiator, Gammatron model, with a dose rate of 97.3 mGy/min at a distance of 10 cm from the source. High doses in the region of hundreds of Gy up to kGy were performed on a gamma-cell type source with a dose rate of 0.380 kGy/h (at the time of irradiation). Irradiations with both ^{60}Co sources were performed at room temperature and under electronic equilibrium conditions.

3. Results and discussion

3.1. X-ray diffraction studies

XRD studies were used to reveal the nature of the crystallinity of the sample synthesized and calcined at 1200 °C for 2 h. Fig. 1(a) shows the diffractogram of the CSO phosphor calcined at 1200 °C, together with the calcium silicate reference standard. Comparing the XRD pattern of the CSO powder sample with the No. 96-900-2180 file of the Match Program, the crystalline peaks are identified as belonging to calcium silicate corresponding to the pseudo-wollastonite phase, as shown in Fig. 1(a). Based on this result, we can confirm the validity of the methodology used to obtain calcium silicate. Fig. 1(b) depicts the monoclinic crystal structure of CSO phosphor designed by VESTA software. The lattice parameters are a = 5.5104 Å, b = 6.7507 Å, c = 10.4354 Å, α = γ = 90.00°, β = 117.23°, and crystalline size 107 nm.

3.2. Thermoluminescence studies

3.2.1. Effect of the thermal treatment

It is known that heat treatment of the material below the melting temperature can modify the shape of the TL glow curve and the intensity of the peaks (González et al., 2013; Bizarri and Moine, 2005). Therefore, in this work, before studying the TL properties of the material, the effect of heat treatment on the TL glow curve of CSO samples has been investigated.

Fig. 2 shows the TL glow curves after annealing the CSO sample at different temperatures of 1100, 1200, and 1300 °C for 2 h. Each annealed sample was irradiated at a dose of 3.5 Gy prior to TL reading. It is observed that the properties of the TL peaks of the CSO sample are slightly changed in their position and significantly changed in their intensity after annealing. For the TL glow curve corresponding to 1100 and 1300 °C annealing, it is observed that the TL peak around 120 and 110 °C are of higher intensity than the other two peaks, respectively. On the other hand, the TL glow curve of the sample annealed at 1200 °C shows a TL peak of higher intensity around 190 °C, and it is 6.0 and 4.6 times more intense than the samples calcined at 1100 and 1300 °C, respectively. Therefore, for the studies to follow we use the sample calcined at 1200 °C. Furthermore, for possible practical application, a stable TL peak above 200 °C is desirable.

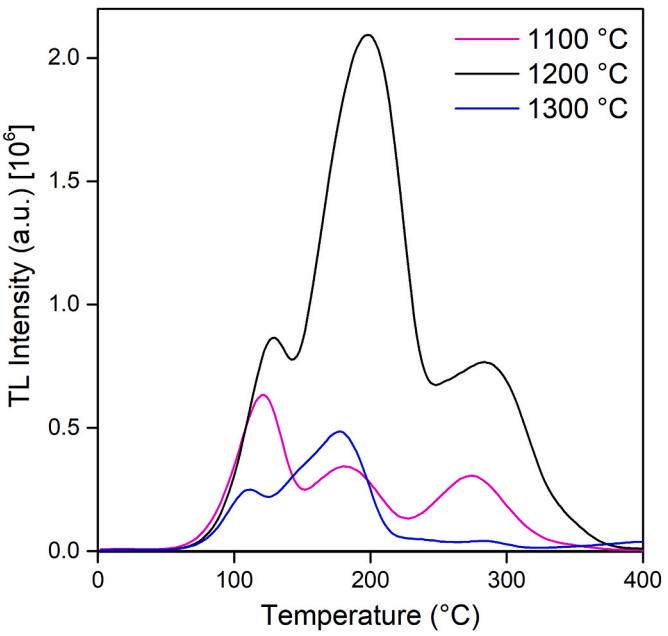

Fig. 2. Glow curve of CSO phosphor samples calcined at temperatures of 1100, 1200, and 1300 °C for 2 h. The samples were irradiated with a dose of 3.6 Gy before TL reading.

3.2.2. Fading

The possible fading effects of the TL response of CSO phosphor due to storage conditions is an important parameter that needs to be determined. For this study, the phosphor CSO pellets were irradiated with a dose of 1 Gy and then stored in the dark with a red light at room temperature (20–25 °C), remaining in this condition for 30 days. The fading of the phosphor CSO for the peak at 120, 190, and 280 °C was calculated as the area under the region of interest (ROI) for temperatures between

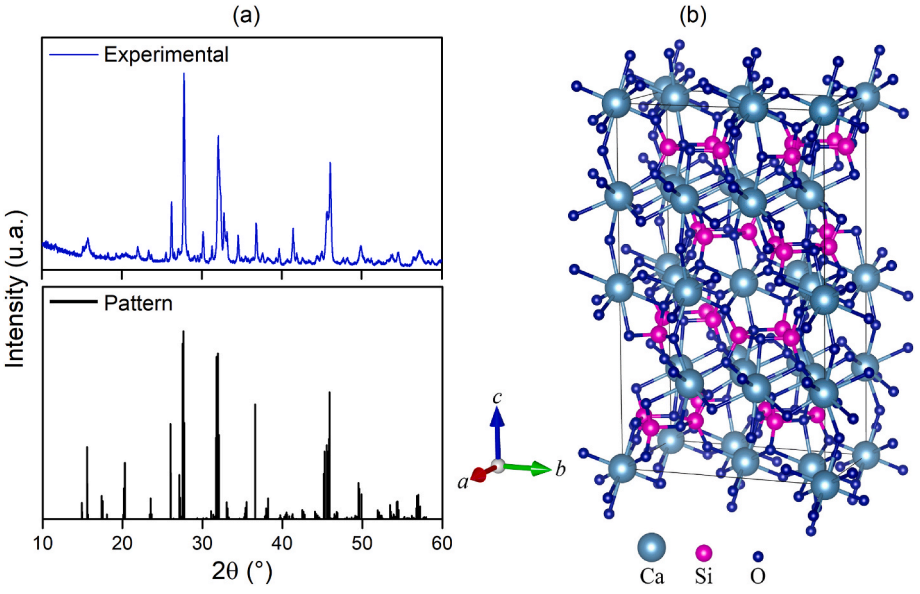

Fig. 1. (a) XRD patterns of CSO phosphor calcined at 1200 °C for 2 h along with the standard spectrum of calcium silicate. (b) The crystal structure of CSO phosphor.

50 and 135 °C, between 135 and 230 °C and between 230 and 330 °C, respectively. Fig. 3 shows the fading of the TL intensity of the peaks at 120, 190 and 280 °C. The inset of Fig. 3 shows the glow TL curve of the CSO phosphor irradiated at 1 Gy and the regions of interest ROI-1, ROI-2, and ROI-3 corresponding to the peaks at 120, 190, and 280 °C, respectively. The TL intensity of each TL peak was normalized to the TL response obtained immediately after irradiation of the CSO phosphor. The peak at 120 °C showed a greater fading of the TL response with a loss of up to 80% of the TL signal after approximately two days (44 h) of storage. However, the TL peaks at 190 and 280 °C remained constant with a slight 8% decay of TL intensity in the first 5 h. Thus, it is concluded that the TL peak at 120 °C corresponds to more unstable or shallower traps in this material, making the probability of recombination higher at room temperature. On the other hand, the two TL peaks at 190 and 280 °C correspond to deep traps with good thermal stability. The TL maxima at 280 °C could arise from the recombination of holes released from the O^- ion (center II) during TL readout with unknown centers that act as electron traps. Similarly, the TL maxima at 280 °C could be linked to the F^+ center (center III) that releases electrons during heating and the subsequent recombination of these electrons with unknown hole trap centers. It was not possible to detect any defect centers in the present study that could be linked to the TL glow peaks maxima at 120 °C, and 190 °C. For a period further than the time analyzed, no additional fading was obtained for the three TL peaks, as shown in Fig. 3. This result allows establishment applications of the CSO phosphor in radiation dosimetry using the TL peak at 190 and 280 °C.

3.2.3. Dose response

Due to the high fading of the peak at 120 °C, the phosphor CSO pellets were preheated at 100 °C for 10 s in the same tray of the TL reader in order to empty the surface traps responsible for the unstable luminescence at low temperatures. TL measurements were performed immediately after this procedure. After being exposed to γ-radiation doses between 20 mGy up to 5 Gy, the samples of the CSO phosphor show two TL glow peaks at around 190 °C and 280 °C (see Fig. 4). The glow peak at 190 °C is more prominent, while the peak at 280 °C has a relatively lower intensity. It is clearly observed in the inset of Fig. 4 that

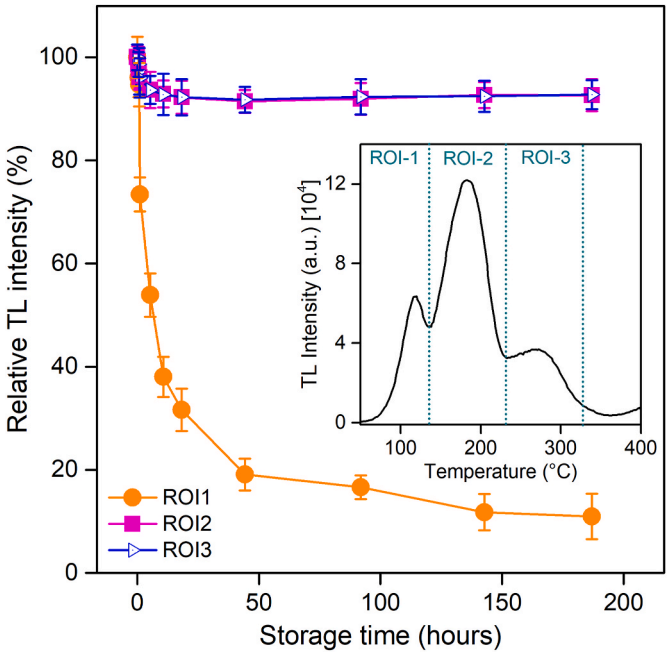

Fig. 3. Normalized TL fading of peaks at 120, 190, and 280 °C as a function of storage time interval. In the inset, deliminations of the three regions of interest in the TL glow curve of the CSO phosphor.

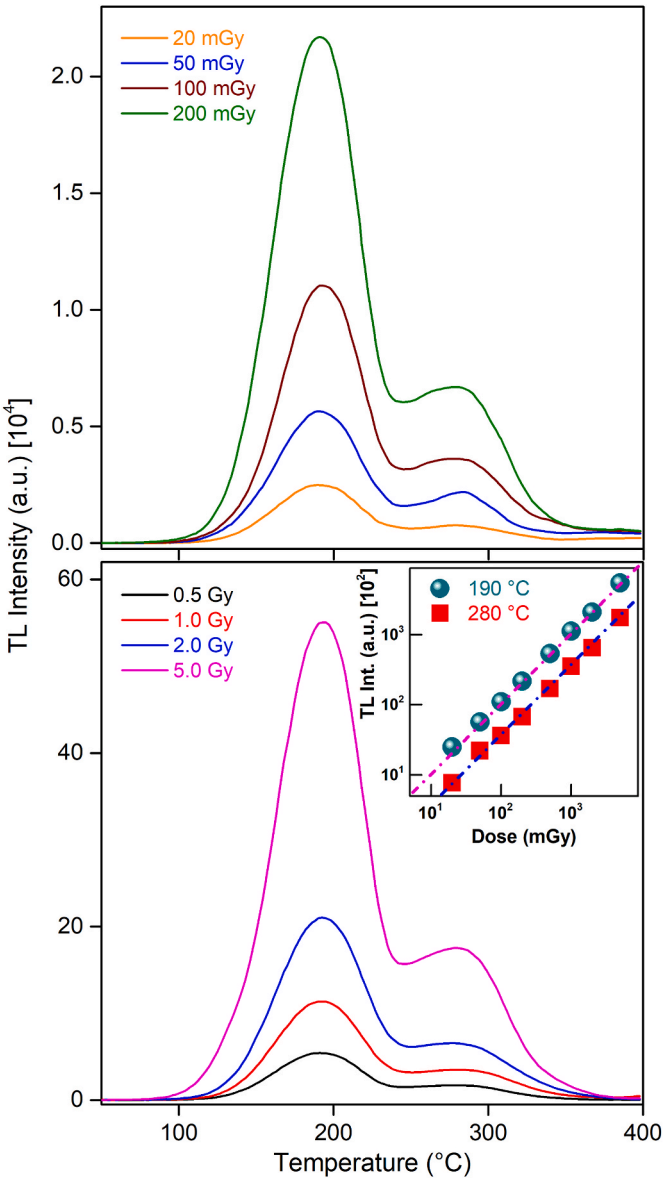

Fig. 4. TL glow curves of CSO phosphor irradiated with γ-radiation doses from 20 to 200 mGy (top) and from 0.5 to 5 Gy (bottom). Inset: intensity variation of TL peak at 190 and 280 °C as a function of γ-irradiation dose. Both axes are presented in logarithmic scale for a better representation of the data. Pink- and blue-dashed lines indicate linearity.

both lines (blue- and pink-spaced lines) are parallel, indicating that both TL peaks at 190 and 280 °C present a linear response in the analyzed dose range. Souza et al. (2007a,b) observed similar behavior for pellets of calcium silicate-Teflon composite. The linear behavior of TL intensity with a dose of CSO phosphor sintered at 1200 °C and a low fading of the TL signal show the potential usefulness of this material in the detection of radiation in the order of mGy in the field of personal and environmental dosimetry.

3.2.4. TL emission spectrum

Fig. 5 shows the 3D TL emission spectrum of CSO phosphor irradiated with a β-radiation source of 6.73 Gy at room temperature. This result shows that the shape and position of the TL peaks are similar to the TL glow curve obtained with γ-radiation. The TL emission spectrum of CSO phosphor presents a band in the range of 250–550 nm centered at 370 nm.

EPR experiments in the present study have detected two defect

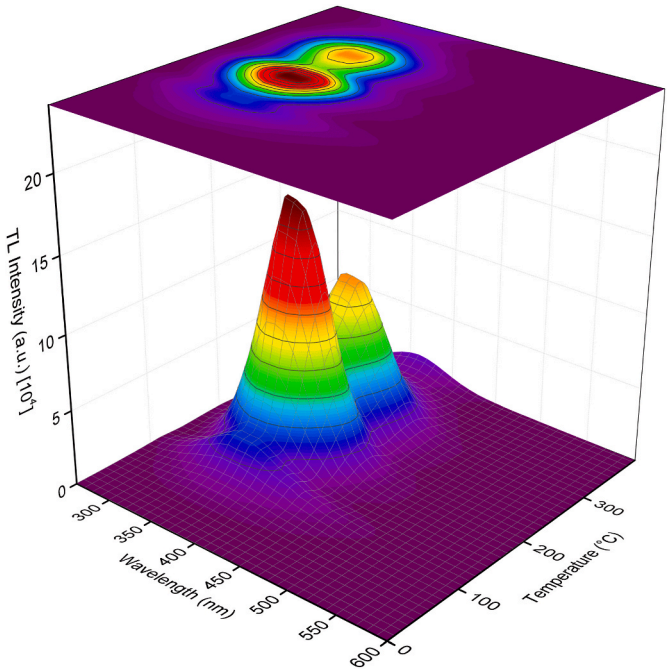

Fig. 5. TL emission spectra of the CSO phosphor measured for a dose of 6.73 Gy. 3D representation (bottom) and contour plot (top).

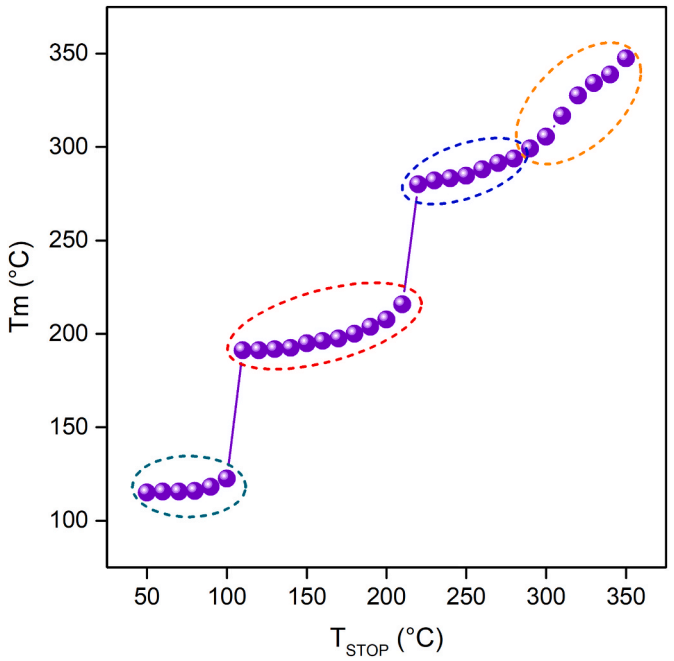

Fig. 6. Tm-Tstop plot of CSO sample. The temperature range regions corresponding to the four TL peaks are indicated.

centers that are found to be associated with the TL peak at 280 °C. Centers that could relate to the low-temperature TL peak at 120 °C, the TL peak at 190 °C, and the recombination center could not be observed in the EPR experiments. Nevertheless, the broad emission band centered at 370 nm results from the charges released from the observed defect centers and also from the centers that could not be detected.

3.2.5. *Tm-Tstop*

Information on the kinetic parameters of the TL glow curve peaks, such as the activation energy, the frequency factor, and the order of kinetics associated with each TL peak is important for the characterization of a new TL material. To determine the kinetic parameters of the experimental glow curve of CSO phosphor, initially, an analysis of the number of peaks and the order of kinetics of each peak was performed using the Tm-Tstop method (McKeever, 1980, 1985).

Fig. 6 shows the Tm-Tstop curve, in which we can observe three regions with behaviors that differ from each other. For the first region between Tstop temperatures from 50 to 100 °C, the Tm-Tstop curve presents a plateau, indicating the presence of a peak with first-order kinetics. For the second region corresponding to Tstop temperatures between 110 and 210 °C, a linear behavior with a slight slope is observed. This result indicates the presence of a peak with kinetics of order different from 1. On the other hand, the third region between Tstop temperatures of 220 and 350 °C presents two subregions, evidencing the presence of at least two superimposed peaks.

The invariance of the TL peak position as a function of dose (see Fig. 4) and the behavior of the Tm-Tstop curve for the third region indicate the presence of at least two TL peaks that obey a continuous distribution of charge carrier traps with first-order kinetics.

3.2.6. *Deconvolution and calculation of kinetic parameters*

With the preliminary results of the Tm-Tstop method, and using the deconvolution method (Benavente et al., 2019), we determined the kinetic parameters of each TL peak of the glow curve of the material.

Fig. 7 shows the result of the deconvolution of the glow curve for the CSO sample irradiated with a γ-radiation dose of 0.539 Gy. Similar results were obtained for other γ-radiation doses (0.067, 0.135, 0.269, 0.404, 0.539, 0.674, 1.347 and 3.368 Gy). The kinetic parameters

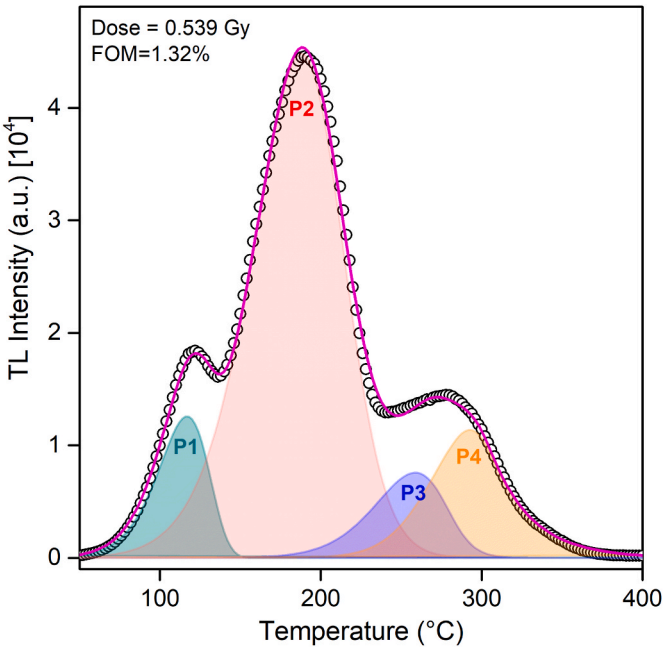

Fig. 7. Deconvolution of the whole glow curve of the CSO phosphor irradiated with 0.539 Gy of γ-radiation. Circles correspond to experimentally collected data and the calculated glow curve (full line in pink) can be achieved by assuming the presence of four peaks. (For interpretation of the references to colour in this figure legend, the reader is referred to the web version of this article.)

obtained from the deconvolution for each γ-irradiation dose are shown in Table 1. For all TL curves, deconvolution evidenced the presence of four overlapping peaks at 117, 190, 252, and 278 °C. The mathematical model used to fit the experimental result of the TL glow curves is based on a linear combination of four functions. This approach aligns with the results of the Tm-Tstop method (Benavente et al., 2020), which indicates that the peaks at 117 and 190 °C correspond to a distribution of localized

Table 1
Details of activation energy (E), maximum temperature (T), frequency factors (s), order of kinetics (b) and distribution width (σ) of the TL peaks of the CSO phosphor obtained by the deconvolution method of the glow curves for different doses. Bottom: the average and coefficient of variation (CV).

Dose (Gy)	FOM	Peak 1: FOK (Discrete)			Peak 2: GOK (Discrete)				Peak 3: FOK (Continuous)				Peak 4: FOK (Continuous)			
		E (eV)	T (°C)	s (s^{-1})	E (eV)	T (°C)	b	s (s^{-1})	E (eV)	T (°C)	σ (eV)	s (s^{-1})	E (eV)	T(°C)	σ (eV)	s (s^{-1})
0.067	1.35%	0.808	118	$6.28{\cdot}10^{9}$	0.692	189	1.186	$5.17{\cdot}10^{6}$	1.346	254	0.0155	$1.70{\cdot}10^{12}$	1.528	277	0.0652	$2.32{\cdot}10^{13}$
0.135	1.24%	0.814	119	$6.92{\cdot}10^{9}$	0.689	191	1.195	$4.48{\cdot}10^{6}$	1.308	255	0.0145	$6.73{\cdot}10^{11}$	1.522	279	0.0663	$1.82{\cdot}10^{13}$
0.269	1.29%	0.800	121	$3.97{\cdot}10^{9}$	0.696	194	1.190	$4.79{\cdot}10^{6}$	1.278	254	0.0152	$3.60{\cdot}10^{11}$	1.534	280	0.0698	$2.23{\cdot}10^{13}$
0.404	1.40%	0.783	119	$2.70{\cdot}10^{9}$	0.700	191	1.185	$6.06{\cdot}10^{6}$	1.253	250	0.0198	$2.48{\cdot}10^{11}$	1.552	278	0.0712	$3.66{\cdot}10^{13}$
0.539	1.32%	0,807	117	$6.59{\cdot}10^{9}$	0.692	188	1.241	$5.50{\cdot}10^{6}$	1.150	252	0.0179	$2.13{\cdot}10^{10}$	1.549	276	0.0772	$3.87{\cdot}10^{13}$
0.674	1.41%	0.784	118	$2.96{\cdot}10^{9}$	0.699	190	1.252	$6.29{\cdot}10^{6}$	1.255	253	0.0164	$2.18{\cdot}10^{11}$	1.550	280	0.0630	$3.16{\cdot}10^{13}$
1.347	1.33%	0.812	114	$9.57{\cdot}10^{9}$	0.682	185	1.241	$4.86{\cdot}10^{6}$	1.311	252	0.0162	$8.34{\cdot}10^{11}$	1.533	276	0.0619	$2.86{\cdot}10^{13}$
3.368	1.57%	0.769	114	$2.40{\cdot}10^{9}$	0.682	186	1.196	$4.70{\cdot}10^{6}$	1.169	250	0.0182	$3.46{\cdot}10^{10}$	1.480	275	0.0678	$9.35{\cdot}10^{12}$
Average		0.79(6)	116.9(6)	$4.70{\cdot}10^{9}$	0.69(3)	189.0(6)	1.21(6)	$5.08{\cdot}10^{6}$	1.25(9)	252.5(4)	0.02(1)	$4.60{\cdot}10^{11}$	1.53(6)	277.5(5)	0.07(2)	$2.40{\cdot}10^{13}$
CV%		3%	3%	–	1%	1%	2%	–	5%	1%	9%	–	2%	1%	7%	–

(discrete) trap values that obey first-order and general-order kinetics with b values closed to 1.2, respectively. On the other hand, the peaks at 252 and 278 °C obey first-order kinetics with continuous trap distribution. The fit between the data was verified by the figure of merit (FOM) (Balian and Eddy, 1977), showing values lower than 1.57%.

3.3. EPR studies

The room temperature electron paramagnetic resonance (EPR) spectrum of γ-irradiated CSO phosphor is shown in Fig. 8. The spectrum arises from three defect centers which are labeled in Fig. 8. Center I has a rhombic g-tensor with principal values 2.014, 2.011, and 2.0080. The center displays hyperfine splitting arising from the interaction of the unpaired electron with three equivalent nuclei with ½ spin. The four lines seen in Fig. 8 are the result of this interaction. The hyperfine splitting is estimated to be about 41 Gauss. Thermal annealing studies have determined the inference that the spectrum results from three defect centers.

In the calcium silicate structure described in the introduction section, there is a possibility of the existence of antisite cation exchange (Kuklja, 2000) in CSO crystal. This cation exchange results in the partial occupancy of Ca^{2+} sites by Si^{4+} ions. Antisite cation exchange is also known as cation exchange disorder and is considered a point defect in crystal systems. Theoretical calculations have predicted their occurrence (Kuklja, 2000) in a crystal lattice. They have also been observed experimentally by Truong et al. (2013). This disorder results in the formation of vacancies in the lattice.

Trapping sites for electrons and holes can be created in a crystal due to antisite disorder. One of the most likely defects formed in this case is the O^- ion, which is a positive hole localized on an oxygen ion near a cation vacancy. Further, γ-irradiation can cause an electron to be trapped at an anion vacancy, forming F^+ centers. Yuan et al. (2015) have demonstrated that anion vacancies can easily form in a lattice with cation disorder.

O^- ions, on the other hand, can be formed by trapping holes at cation

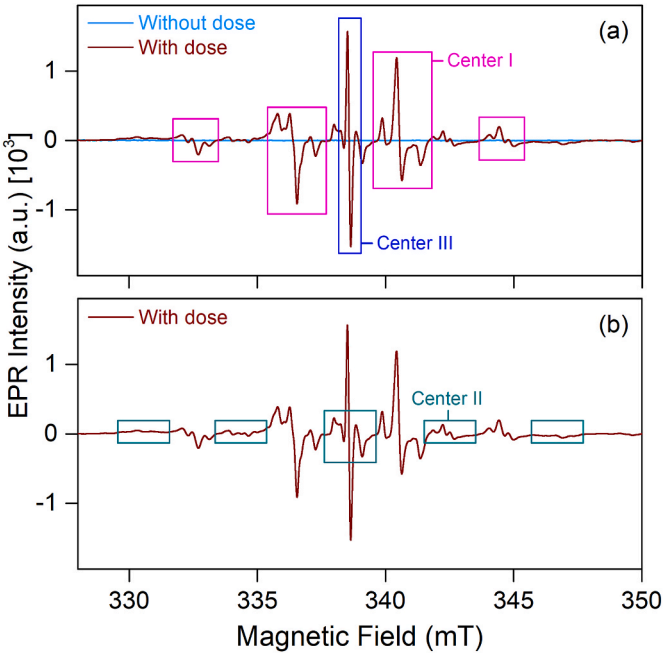

Fig. 8. (a) Room temperature EPR spectrum of γ-irradiated CSO phosphor (γ-dose: 10 kGy). The four pink rectangles show the lines from Center I. These lines are from an O^- ion. Center III is attributed to an F^+ center (blue rectangle). (b) The five lines from center II are shown in green rectangles. Center II is assigned to an O^- ion. (For interpretation of the references to colour in this figure legend, the reader is referred to the web version of this article.)

vacancies (Holston et al., 2015). The stability of the hole is provided by nearby cation vacancies through electrostatic attraction. The hole resides in an oxygen *p*-orbital in an O^- ion and exhibits positive *g*-shifts. Center I in the present study displays a rhombic *g*-tensor and it is observed that all three principal values show positive *g*-shifts. Based on the relatively large *g*-shifts, center I is tentatively identified as the O^- ion. O^- ion normally exhibits an axial *g*-tensor with the parallel component close to the free-spin value (2.0023) and the perpendicular component greater than the free-spin value (Williamson et al., 1971). However, there are systems where O^- ion has a rhombic *g*-tensor as observed in anatase nanoparticles (Misra, et al., 2016). The principal g-values are $g_x = 2.0$, $g_y = 2.01$, and $g_z = 2.03$. Another example is SiO_2 studied by Stapelbroek et al. (1979). Here also, a rhombic *g*-tensor is exhibited by the hole-trapped oxygen ion. On the other hand, the ion also displays an isotropic *g*-value as in $MgAl_2O_4$ (Ibarra et al., 1991). The identification of center I as O^- ion is mainly based on the above findings and the observations of Ibarra et al. (991).

The stability of center I was determined using the pulse-thermal annealing method. The sample was heated to a specific temperature and held at that temperature for 3 min before being cooled to room temperature for EPR measurements. Fig. 9 illustrates the thermal annealing behavior of center I. Center I becomes unstable around 60 °C and undergoes decay in the temperature range of 60 °C–160 °C. No specific TL role could be assigned to this center.

The center labeled as Center II in Fig. 8 exhibits a rhombic *g*-tensor with principal values 2.015, 2.013, and 2.010. Similar to center I, center II displays five hyperfine lines (Fig. 8) with hyperfine splitting equal to 45 Gauss. These five lines result from the interaction of the unpaired spin with nearby four equivalent nuclei with spin ½. Based on the reasons mentioned earlier for the center I assignment, center II is also tentatively attributed to the O^- ion. The thermal annealing behavior of center II is shown in Fig. 9. It is seen that there are two stages where the intensity of the EPR lines decreases. The first stage is from about 60 °C to 175 °C and most probably results from the recombination of charges released elsewhere from unknown defect centers with the hole on the O^- ion. The second stage is from about 230 °C to 350 °C and represents the actual decay of center II. This stage of decay relates to the TL peak at 280 °C and it is inferred that this center correlates with this TL peak.

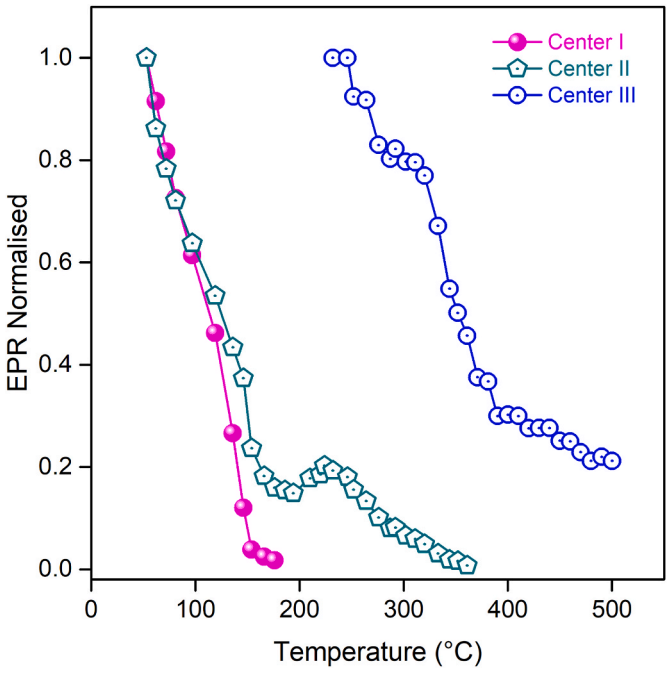

Fig. 9. Thermal annealing behavior of center I (O^- ion), center II (O^- ion), and center III (F^+ -center) in $CaSiO_3$ phosphor.

An F^+ center is a defect center that can form in an oxide system like calcium silicate, where an electron is trapped at an oxygen vacancy. In its first study in an alkali halide (Hutchison, 1949), the center displayed a relatively large linewidth of about 100 Gauss. The center's main characteristic feature is the *g*-value close to the free-electron value of 2.0023. The intrinsic linewidth of the center is quite small and is in the range of one Gauss (Wertz et al., 1957).

The amount of delocalization of the unpaired electron and its interaction with nearest neighbor ions determines the observed linewidth. The linewidth also depends on the magnetic moments of the nuclei of the neighboring ions and the relative abundance of the isotopes of the ions. In alkali halides, where large line widths have been observed, the unpaired electron interacts not only with the immediate neighbors but also with alkali and halide ions in successive neighboring shells (Holton and Blum, 1962).

An anion vacancy captures an electron during irradiation and results in the formation of the F^+ center. The F^+ center exhibits both positive and negative *g*-shifts. The *g*-value of center III is 2.0011 and the *g*-shift is small. The linewidth of the center is 2 Gauss. On the basis of these observed features, center III is tentatively assigned to an F^+ center. The thermal annealing behavior of the center is shown in Fig. 9. It is observed that the center becomes unstable around 240 °C and decays in the temperature range 240 °C–400 °C. It is suggested that center III correlates with the TL peak at 280 °C.

The deconvolution of the experimentally observed TL glow curve has shown the presence of four overlapping peaks at 117, 190, 252, and 278 °C. An examination of the thermal annealing behavior of the centers indicates that centers II and III are linked to the TL maxima at 252, and 278 °C of the deconvoluted glow curve. The physicochemical processes are the same as the ones mentioned for the observance of the experimentally observed TL peak at 280 °C.

4. Conclusion

CSO phosphor was successfully synthesized by the sol-gel method. XRD studies verify the crystallinity of the material as calcium silicate in its so-called pseudo-wollastonite phase. TL sensitivity optimization shows the best results for CSO phosphors sintered at 1200 °C. The CSO phosphor sintered at 1200 °C exhibited three TL peaks at 120, 190, and 280 °C. The TL emission spectrum of CSO phosphor showed a broad band centered at 370 nm. The TL intensity of the peaks at 190 and 280 °C increases linearly with increasing γ-dose between 20 mGy and 5 Gy. The activation energy (E), frequency factor (s), and kinetic order have been estimated using Tm-Tstop and deconvolution methods, revealing four TL peaks. γ-irradiation is found to induce three defect centers in the CSO phosphor. A tentative assignment has been made of the centers to O^- ion, and F^+ center. O^- ion (center II) is suggested to be associated with the TL peak at 280 °C. The F^+ center appears to be also linked to the 280 °C TL peak.

CRediT authorship contribution statement

Zaida V. Vilca: Methodology, Investigation. **T.K. Gundu Rao:** Writing – original draft, Validation, Investigation, Formal analysis, Conceptualization. **René R. Rocca:** Investigation. **J.F. Benavente:** Software, Methodology, Investigation, Writing – review & editing. **Joseff R. Mejia-Bernal:** Investigation. **José F.D. Chubaci:** Investigation. **Betzabel N. Silva-Carrera:** Investigation, Methodology. **Jorge S. Ayala-Arenas:** Methodology, Investigation, Funding acquisition. **Nilo F. Cano:** Writing – original draft, Supervision, Methodology, Investigation, Formal analysis, Conceptualization, Funding acquisition, Writing – review & editing, Data curation.

Declaration of competing interest

The authors declare that they have no known competing financial

interests or personal relationships that could have appeared to influence the work reported in this paper.

Data availability

The data that has been used is confidential.

Acknowledgments

The authors would like to express thanks to Ms. E. Somessari from the Institute for Energy and Nuclear Researches (IPEN), Brazil, for kindly carrying out the γ-irradiation of the samples. This work was supported by PROCIENCIA-CONCYTEC, Peru, in the framework of the call E041-2023-01 (Process number PE501082822-2023 - PROCIENCIA).

References

Balian, H.G., Eddy, N.W., 1977. Figure of merit (FOM), an improved criterion over the normalised chi-squared test for assessing goodness-of-fit of gamma ray spectra peaks. Nucl. Instrum. Methods 145, 389–395. https://doi.org/10.1016/0029-554X(77)90437-2.

Barbosa, R.F., Cano, N.F., Watanabe, S., Guttler, R.A.S., Reichmann, F., 2014. Thermoluminescence in two varieties of jadeite: irradiation effects and application to high dose dosimetry. Radiat. Meas. 71, 36–38. https://doi.org/10.1016/j.radmeas.2014.05.002.

Benavente, J.F., Gómez-Ros, J.M., Correcher, V., 2020. Characterization of the thermoluminescent glow curve of $Li_2B_4O_7$:Cu,Ag. Radiat. Meas. 137, 106427 https://doi.org/10.1016/j.radmeas.2020.106427.

Benavente, J.F., Gómez-Ros, J.M., Correcher, V., 2021. A kinetic model for the thermoluminescent high dose response of LiF:Mg,Cu,P (MCP-N). Appl. Radiat. Isot. 170, 109634 https://doi.org/10.1016/j.apradiso.2021.109634.

Benavente, J.F., Gómez-Ros, J.M., Romero, A.M., 2019. Thermoluminescence glow curve deconvolution for discrete and continuous trap distributions. Appl. Radiat. Isot. 153, 108843 https://doi.org/10.1016/j.apradiso.2019.108843.

Bizarri, G., Moine, B., 2005. On $BaMgAl_{10}O_{17}:Eu^{2+}$ phosphor degradation mechanism: thermal treatment effects. J. Lumin. 199–213. https://doi.org/10.1016/j.jlumin.2004.09.119, 2005.

Cano, N.F., Aynaya-Cahui, S.C., Vilca, Z.V., Rocca, R.R., Gundu Rao, T.K., Silva-Carrera, N.B., Lopez-Gonzales, A.H., Javier-Ccallata, H.S., Ayala-Arenas, J.S., 2023. Preparation and study of the main dosimetric properties by TL of sintered lithium silicate pellets. J. Lumin. 255, 119580 https://doi.org/10.1016/j.jlumin.2022.119580.

Gonzales-Lorenzo, C.D., Ananchenko, D.V., Nikiforov, S.V., Kiryakov, A.N., Zatsepin, A. F., Chubaci, J.F.D., Cano, N.F., Ayala-Arenas, J.S., Watanabe, S., 2021. Effect of 130 keV pulsed electron irradiation on the efficiency of radiative transitions in Eu-doped glass-ceramics $CaSiO_3$. Opt. Mater. 119, 111304 https://doi.org/10.1016/j.optmat.2021.111304.

Gonzales-Lorenzo, C.D., Gundu Rao, T.K., Cano, N.F., Silva-Carrera, B.N., Rocca, R.R., Cuevas-Arizaca, E.E., Ayala-Arenas, J.S., Watanabe, S., 2020. Thermoluminescence and defect centers in β-$CaSiO_3$ polycrystal. J. Lumin. 217, 116783 https://doi.org/10.1016/j.jlumin.2019.116783.

Gonzales-Lorenzo, C.D., Watanabe, S., Cano, N.F., Ayala-Arenas, J.S., Bueno, C.C., 2018. Synthetic polycrystals of $CaSiO_3$ un-doped and Cd, B, Dy, Eu-doped for gamma and neutron detection. J. Lumin. 201, 5–10. https://doi.org/10.1016/j.jlumin.2018.04.037.

González, P.R., Cruz-Zaragoza, E., Furetta, C., Azorín, J., Alcántara, B.C., 2013. Effect of thermal treatment on TL response of CaSO4:Dy obtained using a new preparation method. Appl. Radiat. Isot. 75, 58–63. https://doi.org/10.1016/j.apradiso.2013.02.005.

Hesse, K., 1984. Refinement of the crystal structure of wollastonite-2M (parawollastonite). Z. Krist-Cryst Mater. 168, 93–98. https://doi.org/10.1524/zkri.1984.168.14.93.

Holston, M.S., McClory, J.W., Giles, N.C., Halliburton, L.E., 2015. Radiation-induced defects in $LiAlO_2$ crystals: holes trapped by lithium vacancies and their role in thermoluminescence. J. Lumin. 160, 43–49. https://doi.org/10.1016/j.jlumin.2014.11.018.

Holton, W.C., Blum, H., 1962. Paramagnetic resonance of F centers in alkali halide. Phys. Rev. 125, 89–103. https://doi.org/10.1103/PhysRev.125.89.

Hutchison, C.A., 1949. Paramagnetic resonance absorption in crystals colored by irradiation. Phys. Rev. 75, 1769–1770. https://doi.org/10.1103/PhysRev.75.1769.2.

Ibarra, A., Lopez, F.J., Castro, J., 1991. V centers in $MgAl_2O_4$ spinels. Phys. Rev. B 44, 7256. https://doi.org/10.1103/PhysRevB.44.7256.

Jain, A., Seth, P., Tripathi, A., Aggarwal, S., 2022. Investigations of thermoluminescence characteristics of $CaSiO_3$:Yb phosphor irradiated with gamma rays and carbon ion beam. Appl. Radiat. Isot. 186, 110253 https://doi.org/10.1016/j.apradiso.2022.110253.

Kuklja, M.M., 2000. Defects in yttrium aluminum perovskite and garnet crystals: atomistic study. J. Phys. Condens. Matter 12, 2953–2967. https://doi.org/10.1088/0953-8984/12/13/307.

Kulkarni, S., Nagabhushana, B.M., Nagabhushana, H., Murthy, K.V.R., Shivakumara, C., Damle, R., 2011. Synthesis, structural characterization and thermoluminescence properties of β-irradiated wollastonite nanophosphor. T. Indian Ceram. Soc. 70, 163–166. https://doi.org/10.1080/0371750X.2011.10600165.

Marfunin, A., 1979. Spectroscopy: Luminescence and Radiation Centers in Minerals. Springer, Berlin.

McKeever, S.W.S., 1980. On the analysis of complex thermoluminescence glow-curves: resolution into individual peaks. Phys. Status Solidi 62, 331–340. https://doi.org/10.1002/pssa.2210620139.

McKeever, S.W.S., 1985. Thermoluminescence of Solids. Cambridge University Press, London.

Misra, S.K., Andronenko, S.I., Tipkin, D., Freeman, J.H., Somani, V., Prakash, O., 2016. Study of paramagnetic defect centers in as-grown and annealed TiO_2 anatase and rutile nanoparticles by a variable-temperature X-band and high-frequency (236 GHz) EPR. J. Magn. Magn Mater. 401, 495–505. https://doi.org/10.1016/j.jmmm.2015.10.072.

Nijalingappa, T.B., Veeraiah, M.K., Darshan, G.P., Kavyashree, D., Sharma, S.C., Premkumar, H.B., Nagabhushana, H., 2020. Surface adaptation prompted enhanced photo and thermoluminescence properties of Dy^{3+} doped wollastonite nanophosphor. Mater. Chem. Phys. 249, 123070 https://doi.org/10.1016/j.matchemphys.2020.123070.

Palan, C.B., Koparkar, K.A., Bajaj, N.S., Omanwar, S.K., 2016. Synthesis and TL/OSL properties of CaSiO3:Ce biomaterial. Mater. Lett. 175, 288–290. https://doi.org/10.1016/j.matlet.2016.04.006.

Souza, D.N., Melo, A.P., Caldas, L.V.E., 2007a. TL and TSEE response of Wollastonite-Teflon composites in X-ray beams. Nucl. Instrum. Methods 580, 338–341. https://doi.org/10.1016/j.nima.2007.05.170.

Souza, D.N., Melo, A.P., Oliveira, M.G., Caldas, L.V.E., 2007b. Dosimetric characterization of wollastonite-Teflon composites. Phys. Status Solidi C 4, 1175–1178. https://doi.org/10.1002/pssc.200673869.

Stapelbroek, M., Griscom, D.L., Friebele, E.J., Sigel Jr., G.H., 1979. Oxygen-associated trapped-hole centers in high-purity fused silicas. J. Non-Cryst. Solids 32, 313–326. https://doi.org/10.1016/0022-3093(79)90079-6.

Truong, D., Devaraju, M.K., Tomai, T., Honma, I., 2013. Direct observation of antisite defects in $LiCoPO_4$ cathode materials by annular dark- and bright-field electron microscopy. ACS Appl. Mater. Interfaces 5, 9926–9932. https://doi.org/10.1021/am403018n.

Watanabe, S., Cano, N.F., Gundu Rao, T.K., Carmo, L.S., Chubaci, J.F.D., 2015. Radiation dosimetry using decreasing TL intensity in a few varieties of silicate crystals. Appl. Radiat. Isot. 105, 119–122. https://doi.org/10.1016/j.apradiso.2015.07.056.

Wertz, J.E., Auzins, P., Weeks, R.A., Silsbee, R.H., 1957. Centers in magnesium oxide; confirmation of the spin of magnesium-25. Phys. Rev. 107, 1535–1537. https://doi.org/10.1103/PhysRev.107.1535.

Williamson, W.B., Lunsford, J.H., Naccahe, C., 1971. The EPR spectrum of O^- on magnesium oxide. Chem. Phys. Lett. 9, 33–34. https://doi.org/10.1016/0009-2614(71)80174-4.

Yuan, N., Liu, X., Meng, F., Zhou, D., Meng, J., 2015. First-principles study of La_2CoMnO_6: a promising cathode material for intermediate-temperature solid oxide fuel cells due to intrinsic Co-Mn cation disorder. Ionics 21, 1675–1681. https://doi.org/10.1007/s11581-014-1320-z.